Growth of diamond in liquid metal at 1 atmosphere pressure

Yan Gong
Center for Multidimensional Carbon Materials (CMCM), Institute for Basic Science (IBS)
Da Luo (luodarhoda@gmail.com)
Center for Multidimensional Carbon Materials (CMCM), Institute for Basic Science (IBS)
https://orcid.org/0000-0002-9128-6782
Myeonggi Choe
Center for Multidimensional Carbon Materials (CMCM), Institute for Basic Science (IBS)
Won Kyung Seong (one2rang@gmail.com)
Center for Multidimensional Carbon Materials (CMCM), Institute for Basic Science (IBS)
Pavel Bakharev
Center for Multidimensional Carbon Materials (CMCM), Institute for Basic Science (IBS)
Meihui Wang
Center for Multidimensional Carbon Materials (CMCM), Institute for Basic Science (IBS)
Seulyi Lee
UNIST Central Research Facilities (UCRF), Ulsan National University of Science and Technology (UNIST)
Tae Joo Shin
Graduate School of Semiconductor Materials and Devices Engineering, Ulsan National University of Science and Technology (UNIST)
Zonghoon Lee
Center for Multidimensional Carbon Materials (CMCM), Institute for Basic Science (IBS)
Rodney S. Ruoff (ruofflab@gmail.com)
Center for Multidimensional Carbon Materials (CMCM), Institute for Basic Science (IBS)
https://orcid.org/0000-0002-6599-6764

Research Article

Keywords:

Posted Date: July 5th, 2023

DOI: https://doi.org/10.21203/rs.3.rs-3130239/v1

Abstract

Natural diamonds were (and are) formed (some, billions of years ago) in the Earth's upper mantle in metallic melts in a temperature range of 900–1400°C and at pressures of 5–6 GPa[1,2]; indeed, diamond is thermodynamically stable under high pressure and high temperature (HPHT) conditions as per the phase diagram of carbon[3]. Scientists at General Electric invented and used a HPHT apparatus in 1955 to synthesize diamonds from melted iron sulfide at about 7 GPa and 1600°C[4–6]. There is an existing paradigm that diamond can be grown using liquid metals only at both high pressure (typically 5–6 GPa) and high temperature (typically 1300–1600°C) where it is the stable form of carbon[7]. Here, we describe the growth of diamond crystals and polycrystalline diamond films with no seed particles using liquid metal but at 1 atmosphere pressure, and at 1025°C, breaking this paradigm. Diamond grew at the interface of *liquid metal composed of gallium, iron, nickel, and silicon* and *a graphite crucible*, by catalytic activation of methane and diffusion of carbon atoms in the subsurface region of the liquid metal. Raman spectroscopy with ^{13}C-labeling proves that methane introduced into the growth chamber is the carbon source for many of the regions of newly grown diamond. The new growth diamonds were studied by Raman spectroscopy, scanning and transmission electron microscopy, X-ray diffraction, and photoluminescence. Growth of (metastable) diamond in liquid metal at moderate temperature and 1 atm pressure opens many possibilities for further basic science studies and for the scaling of this type of growth.

Introduction

Diamond, known for being the hardest material, possesses the highest atomic density and thermal conductivity, and a large band gap. When impurities such as N or Si (among other elements) are introduced, it exhibits vacancy centers (color centers) that have sparked interest in magnetic sensing and quantum computing[8,9]. These attributes make diamond a versatile material with a multitude of realized or potential applications, including but not limited to very high-power electronics[10]. The properties of diamond[11] as well as its various applications (both synthetic and natural) have been extensively described in numerous reviews[12,13].

Since synthetic diamonds were made by HPHT in 1955[4] HPHT has been further developed and is currently responsible for approximately 99% of the of synthetic diamonds now produced annually[14]. Carbon dissolved in liquid metal at pressure of 5–6 GPa and temperature of 1300 to 1600°C will add to a seed diamond crystal, and these conditions are milder than for a pure carbon system[7,15]. It is reported that the liquid metal acts as catalyst to dissolve carbon (such as graphite) and as a solvent for this dissolved carbon to diffuse to the diamond seed crystal—while not dissolving the seed crystal or the growing diamond[16]. By employing a temperature gradient under a near-equilibrium process, single crystal diamonds up to one cubic centimeter in size are said to be produced from diamond seed crystals by HPHT growth that takes 5–12 days[15,17,18]. The growth of synthetic single crystal diamonds by HPHT will always be limited to ~ centimeter size due to the components used. We decided some years ago to

explore alternative methods to produce synthetic diamonds under mild conditions including decreasing (particularly) the pressure and also the temperature in the liquid metal, as an intriguing topic for fundamental science: could the existing paradigm be broken?

Liquid metals have many outstanding physical and chemical properties[19,20]. Their liquid surface/interface and the abundancy of electrons and ions offer great opportunities for catalysis[21,22]. However, *all* carbons made to date at 'low pressure' (such as one atmosphere pressure or so) with liquid metals have been graphitic carbons (with very high sp^2-bonded carbon content)[23–28]. Recent studies reported molten metal and/or alloys, including Ni, Pd, and Pt dissolved in Sn, Pb, Bi, In, or Ga, were able to efficiently convert methane to hydrogen and (sp^2-bonded) solid carbon by lowering the activation barrier of breaking the C-H bond[25]. Monolayer or multilayer graphene was reported to be deposited either at the surface of Ga or at the interface between Ga and a substrate when methane was used as carbon precursor[24]. Polymer films that normally do not 'graphitize' were reported to be converted to graphitic carbon at low temperature when contacted by Ga and several alloys[26]. Carbon dioxide was reported to be efficiently converted to (sp^2-bonded) solid carbon through bubbling into the eutectic alloy of gallium and indium at near room temperature[28]. For molten metals with moderate to relatively high solubility (iron, nickel, cobalt, others), only graphite or graphitic carbons are formed (and/or carbides) with them[29–33].

We discovered, and report in detail below, that liquid metal can be used to grow diamond at low pressure. We find that diamond can be grown at the interface of liquid metal and a graphite crucible (and also when the interface is with highly oriented pyrolytic graphite (HOPG) or 'EDM-3 Poco Graphite', each as a thin sheet of material placed at the bottom of the graphite crucible). After rapidly cooling the liquid metal following a growth run in which the liquid metal is exposed to a mixture of methane and hydrogen at 1 atm pressure with no diamond seed particles, we find diamond crystals and/or films that grew on the bottom surface of the liquid metal piece—by observing them on the solidified liquid metal piece that we remove from the crucible.

Our growth of diamond on/in liquid metal at room pressure and modest temperature suggests that a variety of liquid metals are likely to act as solvents and perhaps as catalysts (indium, tin, lead, mercury, bismuth, others) as well. Many other elements can be added to such liquid metals, and we suggest this is likely to result in the synthesis of diamond by nucleation and growth in other liquid metals or at their interface with other materials. It seems likely that solid carbon can also act as a precursor for the growth.

Results and Discussion

Growth of diamond in liquid metal at 1 atm pressure.

Liquid metal containing Ga, Ni, Fe, and Si was used for the growth of diamonds. We used a home-built cold wall vacuum system that can rapidly heat and cool the metal (Fig. 1a). A graphite crucible connected to two water-cooled copper electrodes is joule heated by electrical current at a given voltage (Fig. S1). A pyrometer is connected into a feedback loop and used to measure and control the temperature of the

graphite crucible; its ~ 1-mm diameter laser spot was focused at the center of the outside part of the side of the graphite crucible (Fig. 1b, upper). A small piece of silicon wafer was placed on the bottom of a 20 mm (length) x 10mm (width) x 15 mm (depth) cavity in the crucible and liquid gallium was then added, followed by adding nickel and iron 'ingots' (Fig. 1b (lower) shows this mixture in the cavity prior to heating). A typical growth run was done with the pyrometer reading 1175°C; prior to heating, methane (CH_4) and hydrogen (H_2) were added (after the chamber had been pumped down to the base pressure of its vacuum pump) to reach 760 Torr. Ni, Fe, and Si dissolve entirely into the liquid gallium forming a molten (liquid) metal. The temperature at different regions inside the liquid metal was measured by alumina-sheathed thermocouples, Fig. S2, Table S1-2. We refer to exposure to the methane/hydrogen mixture while heating for a given length of time as a 'growth run'. After a growth run the electrical current was turned off, and the crucible (temperature at the bottom center) cools in about 167 seconds to 25°C (Fig. S3).

Diamonds typically grew in the central region of the bottom surface of this liquid metal alloy, at its interface with either the bottom of the cavity of the graphite crucible, or with thin pieces of HOPG (Grade ZYB, SPI Supplies) or EDM-3 Poco Graphite (0.0190-inch-thick) that we placed at the bottom of the crucible cavity to explore the potential role of different interfaces. A parametric study was undertaken in which these parameters were varied: growth temperatures, the concentrations of Ni, Fe, and Si in liquid Ga (Fig. S4-Fig. S9). We found diamonds were grown in a pyrometer reading temperature range from 1165 ºC to 1190 ºC, and that these diamonds grew most abundantly for a 77.75/11.0/11.0/0.25 mix (atomic percentages) of Ga/Ni/Fe/Si at 1175 ºC during exposure to a gas mixture of methane and hydrogen at 760 Torr that we refer to as an 'optimized growth condition' for growing diamonds and was used for further studies of the growth. When $^{13}CH_4$ was substituted for normal methane, regions with ^{13}C-pure diamonds could be found.

A typical growth result by using the optimized growth condition is shown in Fig. 1c. Diamonds were found on the bottom surface of the solidified Ga-Fe-Ni-Si alloy piece and had "rainbow" colors to the eye (Fig. 1c), and these regions (that were later unequivocally identified as diamond by Raman spectroscopy, transmission electron microscopy (TEM), X-ray diffraction (XRD), by observation of the negatively charged silicon-vacancy (SiV^-) center in diamond, and, for X-ray photoelectron spectroscopy (XPS), by observation of only sp^3-bonded carbon). As mentioned, diamonds nucleate and grow in the center region but not in other regions (some diamond crystals appear to be embedded in the solidified liquid metal surface); we suggest this is because the temperature of this center region (~ 1025 ºC) is the lowest in the liquid metal in the cavity (Fig. S2, Table S1). The diamond size and areal density were highest in the central part of this 'diamond region', and both are reduced as one progresses towards the outermost part of this region (Fig. S10). And, diamonds were only found in the bottom surface of the solidified liquid metal piece (we did not find diamonds on, or embedded in, the 4 sides of the metal piece or its top surface).

Both the size and the density of the diamond crystals increased with time of exposure (the 'growth time') to the methane/hydrogen mixture (Fig. 1d to Fig. 1g) up to 150 min growth time. For a growth time of 15 min, small polyhedral diamond crystals of a low areal density were observed on certain regions (Fig. 1d). For a growth time of 30 min, larger diamond crystals with higher areal density were observed and facets are clearly evident (Fig. 1e). For a growth time of 60 min, the diamond crystals were still larger and had merged together in some regions to form "islands" (Fig. 1f). Some islands with a size of a few microns are shown in Fig. S11. For a growth time of 150 min a nearly continuous diamond film was formed (Fig. 1g). We note that there were a few gaps in the diamond film region (Fig. S12). Scanning electron microscopy (SEM) images of the as-grown diamond with growth times of 15 min, 30 min, and 60 min were acquired at 50.0° tilt and are shown in Fig. S13. When observed in an optical microscope the continuous film shows various colors including red, yellow, and green (Fig. 1h). We note, for growth times longer than 150 min, the thickness and morphology of diamond film did not change (Fig. S14 and Fig. S15).

Characterization of diamond and the solidified liquid metal interface region

The as-grown diamond film can be delaminated and is readily transferrable to other substrate surfaces by dissolving the metal alloy piece using HCl(aq) solution (see Methods). The optical images of the as-transferred diamond film on a Quantifoil holey amorphous carbon film coated Cu TEM grid show it is transparent (Fig. 1i). Atomic force microscopy (AFM) of the as-transferred diamond film on the Cu TEM grid is shown in Fig. 1j and the facets of the diamonds are clearly seen. The plan-view TEM images of the as-transferred diamond film show diamond particles with different sizes and orientations and that there are, in some regions, gaps between the diamond particles (Fig. S16). There was no graphitic structure found in these gaps (Fig. S17). C1s XPS spectrum of an as-transferred film on a 300 nm SiO_2/Si wafer (Inset image in Fig. 1k and Fig. S18) showing a single and symmetric peak at 285.1 eV correlating to sp^3-bonded carbon suggests the film is diamond (Fig. S19)[34]. Synchrotron two-dimensional XRD (2D-XRD) pattern in grazing incidence mode of the same transferred diamond film suggests that it has a cubic structure (Fig. 1k), with (111), (220) and (311) diffraction Debye rings observed, suggesting that the as-transferred diamond film is polycrystalline.

We used $^{13}CH_4$ (99 at% ^{13}C) instead of normal methane (98.9 at% ^{12}C) for some growth runs. We label the as-grown samples as ^{13}C-D150-GC for a 150 min growth run, for the configuration that the entire bottom surface of the crucible cavity was contacted with liquid metal (Fig. 2a). Raman spectrum (all of which were obtained with a 266 nm excitation source) acquired on ^{13}C-D150-GC (Fig. 2b) showed diamond peaks at 1283 cm^{-1} and 1332 cm^{-1}, and graphite G band peaks at 1521 cm^{-1} and 1580 cm^{-1}, which are the Raman bands of essentially pure ^{13}C-labeled diamond (^{13}D) and normal diamond (^{12}D)[35], and the G bands of essentially pure ^{13}C-labeled graphite (^{13}G) and normal graphite (^{12}G)[36], respectively. Such Raman spectrum can be rationalized by both the methane and the graphite crucible contributing

carbon to the growth of diamond and graphite. With the observed much larger intensity of Raman ^{12}D and ^{12}G peaks as compared to ^{13}D and ^{13}G peaks, the graphite crucible seems to contribute larger amounts of carbon for growth of both diamond and graphite, than methane. Observing Raman ^{13}D and ^{12}D peaks (and the ^{13}G and ^{12}G peaks) with no peaks between them was unexpected. We speculate that the diffusion pathways of the carbon species coming from methane and coming from the graphite crucible are perhaps different.

The graphite crucible is composed of isotropic graphite. We asked: could different types of carbon (carbon material) 'interfaced' with the liquid metal, influence diamond growth at this interface? We thus covered regions of the bottom of the cavity with flat (square or rectangular) pieces of different types of graphite than the crucible graphite, among them HOPG pieces and EDM-3 Poco Graphite plates, and here we present results obtained with EDM-3 Poco Graphite (about HOPG, Fig. S20). Placing *one* piece of EDM-3 Poco Graphite plate, or a stack of ten of them, on the bottom surface of the cavity prior to adding the Ga, Fe, Ni, and Si led to as-grown diamonds using $^{13}CH_4$ that we name ^{13}C-D150-EDM and ^{13}C-D150-SEDM ("S" for stacked), see Fig. 2a. Raman spectrum of ^{13}C-D150-EDM showed ^{13}D and ^{12}D peaks (and ^{13}G and ^{12}G peaks) but the intensities of the ^{12}D and ^{12}G peaks were significantly lower compared to that of the ^{13}D and ^{13}G peaks, showing the growth was mainly from $^{13}CH_4$ (that is, from methane). The spectrum of ^{13}C-D150-SEDM showed only ^{13}D and ^{13}G, thus all newly grown carbon was from $^{13}CH_4$. It is thus reasonable to assume that ^{12}D and ^{12}G Raman peaks observed in ^{13}C-D150-EDM were coming from carbon from the graphite crucible rather than the inserted EDM-3 Poco Graphite plate: that is, the EDM-3 Poco Graphite plate does not contribute carbon to the growth of diamond and graphite. The morphologies of ^{13}C-D150-GC, ^{13}C-D150-EDM, and ^{13}C-D150-SEDM were quite similar (Fig. S21). SEM images (Fig. S22) showing that the surface of the graphite crucible is rougher and has larger pores present than EDM-3 Poco Graphite plate possibly rationalizes why some carbon in the crucible contribute to the growth of diamond and graphite.

The intensity ratio of the Raman peaks for diamond and graphite (I_D/I_G) was higher for ^{13}C-D150-SEDM than for ^{13}C-D150-GC or ^{13}C-D150-EDM. Raman maps of the ^{13}D intensity (Fig. S23) and the I_D/I_G ratio (Fig. 2c) of ^{13}C-D150-SEDM show that diamond and graphite formed continuously throughout the mapped region. (The black spots in Fig. 2c are due to cosmic rays incident on the detector during mapping (Fig. 2d)). Essentially similar I_D/I_G peak ratio was also observed for the as-grown diamonds grown with the same configuration with normal methane (Fig. S24).

A typical photoluminescence (PL) spectrum of ^{13}C-D150-SEDM excited by a 532 nm laser is shown in Fig. 2e. The strong peak at 738.5 nm (1.679 eV) with a full width at half-maximum of 6.4 nm can be assigned to the zero-phonon line (ZPL) of the SiV^- color center[37]. A photoluminescence map of ZPL intensity over a 50 μm × 50 μm region showed this ZPL everywhere but with somewhat varying intensity (Fig. 2f).

Cross-sectional TEM analysis was used to study the atomic scale structure and elemental composition of as-grown diamonds, as-grown graphite, and different regions of the solidified liquid metal piece that were interfaced with these solid carbons. The cross-section specimens were prepared by focused ion beam (FIB) milling of the metal pieces from growth times of 150 min (D150) and 30 min (D30) (see Methods). A typical large-area cross-section TEM image of D150 showed a diamond film at the solidified liquid metal surface (Fig. 3a). (We note the growth of diamond was usually accompanied with the growth of graphite in our experimental conditions, and the surface of solidified liquid metal was not always flat. More details are shown in Fig. S25 and Fig. S26.) High-resolution TEM (HR-TEM) images of the diamond-metal interface show that the metal region has two different structures: one (labeled as M1) with a thickness of about 30 nm, while the other (labeled as M2) is interfacing with M1 (Fig. 3b-c). The fast Fourier transform (FFT) patterns of M1 (upper inset) and M2 (lower inset), show that M1 is amorphous but M2 is crystalline (Fig. 3c). M2 shows a crystal lattice with clearly identifiable fringe spacings and without any structural defects or disorder. (While our 'quenching' cooled the liquid metal due to turning off the electric current that had been driving the Joule heating, as described above, it did not "freeze in" the amorphous liquid metal state—crystallization of the interior of the liquid metal did occur in the few tens of seconds time scale of cooling—and without the formation of separated phases.)

The near-surface solidified liquid metal region that is beneath the diamond film was studied by TEM Energy-dispersive X-ray spectroscopy (TEM-EDS) line profiling, by scanning along the surface of M1 to the bulk of M2 (Fig. 3d), and we found a significant amount of carbon (as atoms or very small clusters) is present in the M1 region. The carbon concentration decreases significantly from ~ 26.5 at% at the top surface to ~ 5.0 at% at a depth of ~ 40 nm, that is matched to the thickness of M1, and (seemingly) plateaus at ~ 3.0–5.0 at% for the M2 region. However, the M2 region might be carbon-free as the detection limit of this method of identifying carbon concentration is ~ 2.0–4.0 at%. Thus, a high percentage of carbon is "dissolved" in the M1 region of the (solidified) liquid metal prior to very rapid solidification but not to any, or any appreciable degree, in the bulk of the liquid metal; the presence of such a high concentration of carbon in the M1 region is perhaps the reason for this region being amorphous.

Electron energy loss spectroscopy (EELS) spectra acquired from 20 randomly selected regions over the diamond region show only one major σ* peak around 292 eV (Fig. 3e)[38], suggesting the whole region is a uniform diamond film. Atomic resolution TEM (AR-TEM) image obtained from the diamond region (marked by the yellow cross in Fig. 3b) observed from the [110] zone axis (that is, the beam direction (BD) is [110]) show the region is running parallel to the (110) diamond planes, with the C – C 'dumbbell' units observed as bright spots in Fig. 3f[39,40].

We further imaged the interface between diamond and the (solidified) liquid metal surface at the early stage of growth (D30). Isolated diamond crystals (for example, the one labeled as D1 in Fig. 3g) were found at the interface (Fig. 3g), and this agrees well with the SEM images (Fig. 1e). Amorphous M1 and crystalline M2 regions were again found underneath the diamond crystals (Fig. 3g-h, Fig. S27; we note M1 in some regions was delaminated from M2). TEM-EDS maps of C, Ga, Ni, Fe and Si in the region where

D1 is located were obtained (Fig. S28). TEM-EDS analysis shows the M1 region of D30 is carbon-rich (Fig. S29).

D1 was found to be directly contacting the surface of the M1 region (Fig. 3h). The D1 crystal lattice fringes are not aligned with the same angle to the M1 surface (i.e., there is not a constant orientation between the D1 lattice fringes and the M1 surface; Fig. 3i).

How does diamond grow?

Here, we speculate about how nucleation and growth might progress, based on our experimental results. The formation of a thin carbon rich M1 region suggests that the growth of diamonds was facilitated by surface catalysis and diffusion of carbon atoms in a thin subsurface region of the liquid metal. That is, carbon is present only in this subsurface region of the liquid metal and this carbon leads to the nucleation and growth of diamonds. During the growth at high temperature, Ni, Fe and Si are all dissolved in the Ga solvent and perhaps all 4 elements (or some more than others) contribute to catalytic generation of C atom precursors that grow diamond. The bottom surface of this liquid metal (at the interface between the metal and the graphite crucible) dissolves carbon atoms or C-H radicals from methane and/or the graphite crucible surface, and the concentration of the precursor carbon species likely follows the temperature gradient at the interface (Fig. S30). We speculate that the relevant carbon species diffused from the high temperature regions (the sides of the graphite crucible) to the center regions (of the bottom surface of the molten metal that is at a relatively lower temperature (Fig. S2, Table S1)), to form diamond crystals. Our control experiments with only Ni dissolved in Ga yielded a very thick graphite film on the entire surface of the liquid metal (Fig. S7 and Fig. S9). The formation of graphite was suppressed with Fe dissolved in the liquid metal alloy (Fig. S8 and Fig. S9).

We emphasize that Si plays a critical role in our growth of diamond. Si was also relevant in our prior studies of homoepitaxial growth of diamond on single crystal diamond[41]. 0.25 at% Si used for our typical growth yields the diamonds of largest crystal sizes at 150 min growth. 0.50 at% Si (and 150 min growth) leads to a much higher density growth of diamonds of smaller crystal sizes (Fig. S5 and Fig. S6). These two results along with our observation of the SiV^- color center, suggest Si plays a role in the nucleation of diamond; a higher nucleation density would rationalize the higher density growth of smaller diamonds at 0.50 at%. We note that the absence of Si (per TEM-EDS) in the M1 region correlates with cessation of diamond growth (Fig. S31). For example, Fig. S25 and Fig. S31c-d shows C present in M1 and a graphite layer beneath the diamond film layer—but no Si. We found by AFM measurements essentially the same thickness diamond film for 300 min growth runs vs 150 min growth runs (Fig. S15). (That is: after ~ 150 minutes there is no more Si present, and longer growth runs do not yield more diamond.)

Conclusion

We found a method to grow diamonds at 1 atmosphere pressure and under a moderate temperature by using a liquid metal alloy: this is unprecedented given the paradigm that diamond could only be grown

using liquid metals with pressures in the range of 5–6 GPa (and temperatures in the range of 1300 to 1600°C). The diamond film contains SiV^- color centers and can be transferred to any other substrates. We suggest that straightforward modifications could enable growing diamond over a very large area by using a larger surface/interface, by configuring heating elements to achieve a much larger isothermal region, and by distributing carbon to the diamond growth region in some new ways that we are now exploring with our current (small) growth system.

The general approach of using liquid metals could accelerate and advance the growth of diamonds on a variety of surfaces, and perhaps facilitate the growth of diamond on small diamond (seed) particles. Considering the large number of possibilities for liquid metals, their eutectics, and the possibility of adding different amounts of various other elements that can act as catalysts (e.g., dissolving some cobalt in gallium (Fig. S32) or bismuth—among many other elements that can be tried), the possibilities for exploring diamond growth with this type of approach appear exceptionally promising.

Methods

Growth of diamonds. An as-received graphite crucible (Ibiden Ex-60 graphite that was machined by a shop in Korea (GMPI)) was annealed at 1100 ºC in a mixture of H_2 (99.999 at% from KOGAS Tech, 100 sccm) and Ar (from Korea Noble Gas Co., LTD, 99.999 at%, 5 sccm) gas flow at 1 atm pressure for 8 h (Fig. S33 and Note S1), with the goal of removing impurities; for example our SEM imaging for runs using the unannealed crucibles showed more metal oxides (particularly aluminum and magnesium). The mixture of Ni ingots (iTASCO, 99.995 wt%) or Co ingots (iTASCO, 99.9 wt%), iron ingots (iTASCO, 99.99 wt%), small pieces broken from a single crystal Si wafer (Silicon Technology Corporation), and liquid gallium (Changsha Rich Nonferrous Metals Co., Ltd; 99.9999 wt%) were put into the graphite crucible cavity.

The growth chamber is shown in Fig. S1. The graphite crucible is clamped to two water-cooled electrodes inside the chamber of our home-built cold-wall joule heating system (the walls are water-jacketed with cooling water flowing between them). The system is connected to gases connected to mass flow controllers and a vacuum system. It is pumped down until the chamber pressure reached 2 mTorr; the pump is isolated and 1000 sccm H_2 flowed until the chamber pressure reaches 760 Torr. We then turn on the current to heat the graphite crucible from 25 ºC to the growth temperature at a heating rate of 7.7°C/sec. The temperature at the surface of the center of the outside of the 'long side' of this graphite crucible was monitored and controlled by a pyrometer (Sensor Therm GmbH, Metis M313) with a feedback system that controls the applied current and voltage. When the temperature read by the pyrometer reached the growth temperature, we changed the H_2 flow rate from 1000 sccm to 100 sccm, and simultaneously flowed 5 sccm CH_4 (from Korea Noble Gas Co., LTD, 99.999 at %). The temperature of the crucible and the flow rates of CH_4 and H_2 were held constant for different growth times; then the current was turned off and the crucible rapidly cooled. For ^{13}C-labeling experiments, $^{13}CH_4$ (Cambridge

Isotopes Laboratories, Inc., CLM-429-PK, 99 at% pure) was used instead of the “normal” methane mentioned above.

Diamond film transfer. As-grown diamond film on solidified liquid metal was transferred onto Quantifoil holey amorphous carbon film (R2/1) coated Cu TEM grid (SPI Supplies, 300 mesh), and 300 nm SiO_2/Si wafer pieces for characterization by optical microscopy, AFM, TEM, and XRD. Some of the solidified liquid metal piece after growth were immersed in an 80 ºC heated solution of HCl(aq) (35–37%, Daejung Chemicals & Metals). The diamond films detach from the metal surface and go to the bottom of the aqueous HCl solution. We note that only a very small amount of the solidified liquid metal piece needs to be dissolved to “free” the diamond film regions. Evidently due to the density of diamond, these sink to the bottom of the HCl(aq) solution. The diamond films were transferred into deionized water. After washing the diamond films 3x with deionized water, they were then transferred onto the target substrate, that was then dried at 60 ºC in an oven overnight.

Characterization. SEM images were obtained with an FEI Verios 460. A Zeiss optical microscope (AxioCam MRc5) was used to acquire optical images. AFM data was acquired with a Bruker Dimension Icon system. Synchrotron 2D-XRD pattern in grazing incidence mode of a transferred diamond film on a 300 nm SiO_2/Si wafer was acquired at the PLS-II 6D UNIST-PAL beamline (bending magnet source) of the Pohang Accelerator Laboratory (PAL) using 18.986 keV X-rays. XPS spectra were acquired on the transferred diamond film on the 300 nm SiO_2/Si wafer with a beam size of 200 μm using a Thermo Scientific ESCALAB 250 Xi XPS equipment equipped with an optical microscope, which was used to locate the beam on the diamond film region. Quenching temperature data was acquired with R-type thermocouples (Fig. S3). Visible Raman spectra and UV Raman spectra were obtained using a WITec GmbH instrument with 532 nm laser wavelength excitation focused through a 100x objective at 1 mW, and 266 nm wavelength laser excitation focused through a 40x objective at 15 mW, respectively. UV Raman maps of the as-grown diamond films on the solidified liquid metal surface were acquired with a scan parameter of 1 point per 2 microns over a 50.0 μm × 50.0 μm region at 15 mW. PL spectra and maps were obtained with this WITec GmbH instrument, excited by the 532 nm wavelength laser light focused through a 100x objective. The PL map of the diamond film was acquired with a scan parameter of 1 point per micron over a 50.0 μm × 50.0 μm region. TEM samples for cross-section TEM measurements were prepared using FIB (Helios 450HP SEM-FIB) milling. TEM imaging, TEM-EDS data, EELS spectra, and SAED patterns were obtained using an aberration corrected TEM (FEI Titan G2 60–300) at an acceleration voltage of 80 kV.

Declarations

Data availability

The datasets generated during the current study, and/or analyzed during the current study, are available from the corresponding author upon reasonable request.

Acknowledgements

Supported by the Institute for Basic Science (IBS-R019-D1). The authors thank Su Yong Lee who assisted with data acquisition and offered advice for the microbeam XRD experiments, and Ben Cunning for suggesting the EDM-3 Poco Graphite sheet material and for discussions. The experiments at the PLS-II 6D and 9C beamline were supported in part by MSIT, POSTECH, and UNIST Central Research Facilities.

Author contributions

R.S.R. supervised the project. R.S.R., D.L., and Y.G. conceived the experiments. Y.G. did growth experiments. Y.G. and D.L. characterized diamond samples. W.S. designed, assembled and built, and tested the cold-wall system and the thermocouple probe array. M.C. and Z.L. did the TEM/STEM/EELS/EDX measurements. P.B did XPS measurements. T.J.S. and S.L. did the XRD measurements. M.W contributed through discussion. Y.G. wrote a draft manuscript and R.S.R., D.L. and Y.G. revised it. All coauthors commented on the manuscript prior to its submission.

Competing interests

The Institute for Basic Science has filed a patent application (KR 10-2023-0052752) that lists Y.G., D.L, and R.S.R. as inventors. Other than this, the authors declare no competing interests.

References

1. Haggerty, S. E. Diamond genesis in a multiply-constrained model. *Nature* **320**, 34-38 (1986).
2. Pal'yanov, Y. N., Sokol, A. G., Borzdov, Y. M., Khokhryakov, A. F. & Sobolev, N. V. Diamond formation from mantle carbonate fluids. *Nature* **400**, 417-418 (1999).
3. Bundy, F. P. *et al.* The pressure-temperature phase and transformation diagram for carbon; updated through 1994. *Carbon* **34**, 141-153 (1996).
4. Bundy, F. P., Hall, H. T., Strong, H. M. & Wentorfjun, R. H. Man-Made Diamonds. *Nature* **176**, 51-55 (1955).
5. Bovenkerk, H. P., Bundy, F. P., Hall, H. T., Strong, H. M. & Wentorf, R. H. Preparation of Diamond. *Nature* **184**, 1094-1098 (1959).
6. Hazen, R. M. & Hazen, R. M. *The diamond makers*. (Cambridge University Press, 1999).
7. D'Haenens-Johansson, U. F. S., Butler, J. E. & Katrusha, A. N. Synthesis of Diamonds and Their Identification. *Reviews in Mineralogy and Geochemistry* **88**, 689-753 (2022).
8. Doherty, M. W. *et al.* The nitrogen-vacancy colour centre in diamond. *Physics Reports* **528**, 1-45 (2013).
9. Ruf, M., Wan, N. H., Choi, H., Englund, D. & Hanson, R. Quantum networks based on color centers in diamond. *Journal of Applied Physics* **130** (2021).

10. Shikata, S. Single crystal diamond wafers for high power electronics. *Diamond and Related Materials* **65**, 168-175 (2016).
11. Railkar, T. A. *et al.* A Critical Review of Chemical Vapor-Deposited (CVD) Diamond for Electronic Applications. *Critical Reviews in Solid State and Materials Sciences* **25**, 163-277 (2000).
12. Butler, J. E., Mankelevich, Y. A., Cheesman, A., Ma, J. & Ashfold, M. N. R. Understanding the chemical vapor deposition of diamond: recent progress. *J. Phys.: Condens. Matter* **21**, 364201 (2009).
13. Satoshi Yamasaki, Paulius Pobedinskas & Nicley, S. S. Recent Advances in Diamond Science and Technology. *Phys. Status Solidi A* **214**, 1770167 (2017).
14. Linde, O., Geyler, O. & Epstein, A. The Global Diamond Industry 2018: A Resilient Industry Shines Through. *Tech. Rep., Bain & Company* (2018).
15. Dossa, S. S. *et al.* Analysis of the High-Pressure High-Temperature (HPHT) growth of single crystal diamond. *Journal of Crystal Growth* **609**, 127150 (2023).
16. Ferro, S. Synthesis of diamond. *Journal of Materials Chemistry* **12**, 2843-2855 (2002).
17. Eaton-Magaña, S., Shigley, J. E. & Breeding, C. M. Observations on HPHT-grown synthetic diamonds: a review. *Gems & Gemology* **53**, 262-284 (2017).
18. Sumiya, H., Harano, K. & Tamasaku, K. HPHT synthesis and crystalline quality of large high-quality (001) and (111) diamond crystals. *Diamond and Related Materials* **58**, 221-225 (2015).
19. Kalantar-Zadeh, K. *et al.* Emergence of Liquid Metals in Nanotechnology. *ACS Nano* **13**, 7388-7395 (2019).
20. Taccardi, N. *et al.* Gallium-rich Pd–Ga phases as supported liquid metal catalysts. *Nature Chemistry* **9**, 862-867 (2017).
21. Daeneke, T. *et al.* Liquid metals: fundamentals and applications in chemistry. *Chemical Society Reviews* **47**, 4073-4111 (2018).
22. Camacho-Mojica, D. C. *et al.* Charge Transfer during the Dissociation of H2 and the Charge State of H Atoms in Liquid Gallium. *J. Phys. Chem. C* **123**, 26769-26776 (2019).
23. Ueki, R. *et al.* In-situ observation of surface graphitization of gallium droplet and concentration of carbon in liquid gallium. *Japanese Journal of Applied Physics* **51**, 06FD28 (2012).
24. Fujita, J.-i. *et al.* Near room temperature chemical vapor deposition of graphene with diluted methane and molten gallium catalyst. *Scientific reports* **7**, 12371 (2017).
25. Upham, D. C. *et al.* Catalytic molten metals for the direct conversion of methane to hydrogen and separable carbon. *Science* **358**, 917-921 (2017).
26. Allioux, F.-M. *et al.* Carbonization of low thermal stability polymers at the interface of liquid metals. *Carbon* **171**, 938-945 (2021).
27. Kawasaki, H. *et al.* A liquid metal catalyst for the conversion of ethanol into graphitic carbon layers under an ultrasonic cavitation field. *Chem. Commun.* **58**, 7741-7744 (2022).
28. Zuraiqi, K. *et al.* Direct conversion of CO_2 to solid carbon by Ga-based liquid metals. *Energy & Environmental Science* **15**, 595-600 (2022).

29. Ching Li, P. E. I. Preparation of Single-Crystal Graphite from Melts. *Nature* **192**, 864-865 (1961).
30. Tulloch, H. J. C. & Young, D. A. Synthetic Single Crystals of Graphite. *Nature* **211**, 730-731 (1966).
31. Yoshihiro, S., Masumi, U. & Sadao, S. Formation of Graphite Single Crystal from Iron Solution by the Slow Cooling Method. *Bulletin of the Chemical Society of Japan* **61**, 1577-1585 (1988).
32. Noda, T., Sumiyoshi, Y. & Ito, N. Growth of single crystals of graphite from a carbon-iron melt. *Carbon* **6**, 813-816 (1968).
33. Austerman, S. B., Myron, S. M. & Wagner, J. W. Growth and characterization of graphite single crystals. *Carbon* **5**, 549-557 (1967).
34. Merel, P., Tabbal, M., Chaker, M., Moisa, S. & Margot, J. Direct evaluation of the sp^3 content in diamond-like-carbon films by XPS. *Applied Surface Science* **136**, 105-110 (1998).
35. Chu, C., d'Evelyn, M., Hauge, R. & Margrave, J. Mechanism of diamond growth by chemical vapor deposition on diamond (100),(111), and (110) surfaces: Carbon-13 studies. *Journal of applied physics* **70**, 1695-1705 (1991).
36. Cai, W. *et al.* Synthesis and solid-state NMR structural characterization of 13C-labeled graphite oxide. *Science* **321**, 1815-1817 (2008).
37. Yang, B. *et al.* Fabrication of silicon-vacancy color centers in diamond films: tetramethylsilane as a new dopant source. *CrystEngComm* **20**, 1158-1167 (2018).
38. Feng, Z., Lin, Y., Tian, C., Hu, H. & Su, D. Combined study of the ground and excited states in the transformation of nanodiamonds into carbon onions by electron energy-loss spectroscopy. *Scientific Reports* **9**, 3784 (2019).
39. Luo, K. *et al.* Coherent interfaces govern direct transformation from graphite to diamond. *Nature* **607**, 486-491 (2022).
40. Tulić, S. *et al.* Covalent Diamond–Graphite Bonding: Mechanism of Catalytic Transformation. *ACS nano* **13**, 4621-4630 (2019).
41. Gong, Y. *et al.* Homoepitaxial Diamond Grown in a Liquid Metal Solvent. ChemRxiv. Cambridge: Cambridge Open Engage (2022).

Figures

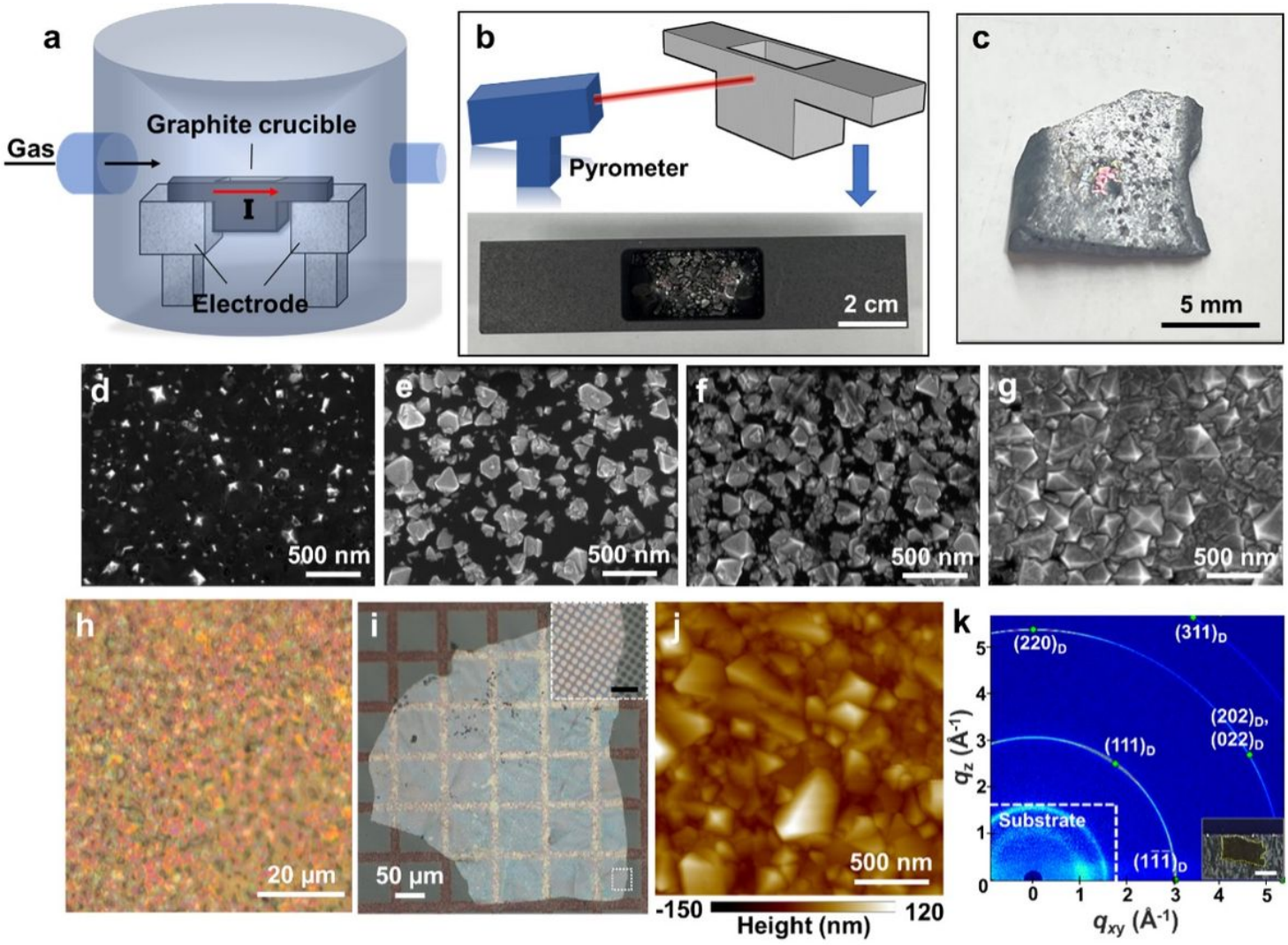

Figure 1

Synthesis of diamond on a liquid metal surface that is at an interface with graphite. (a) Scheme of the experimental setup: A graphite crucible with cavity is the Joule-heated sample container in the cold wall system. (b) (upper) Scheme of the pyrometer and graphite crucible, and (lower) top view photo of the actual graphite crucible after filling the rectangular cavity with Ga, Ni, Fe, and Si. (c) A photo showing the as-grown diamond on the solidified liquid metal surface after a growth run. (d-g) SEM images of diamond crystals after growth for (d) 15 min, (e) 30 min, (f) 60 min, and (g) 150 min. (h) An optical image of the as-grown continuous diamond film on the solidified liquid metal surface. (i) An optical image of the as-transferred diamond film on a Quantifoil holey amorphous carbon film coated Cu TEM grid; Inset (upper right) shows a magnified optical image of the region inside the white dotted lines. The scale bar is 10 μm. (j) AFM topographic image of the as-transferred diamond film on the Cu TEM grid. (k) 2D-XRD pattern of a transferred diamond film on a 300 nm SiO_2/Si wafer silicon wafer. Dotted rectangle region: from the Si substrate and/or double-sided tape. Inset (lower right): The photograph of the transferred diamond film (yellow dotted area) adhered to the wafer with a double side tape; the scale bar is 1 mm.

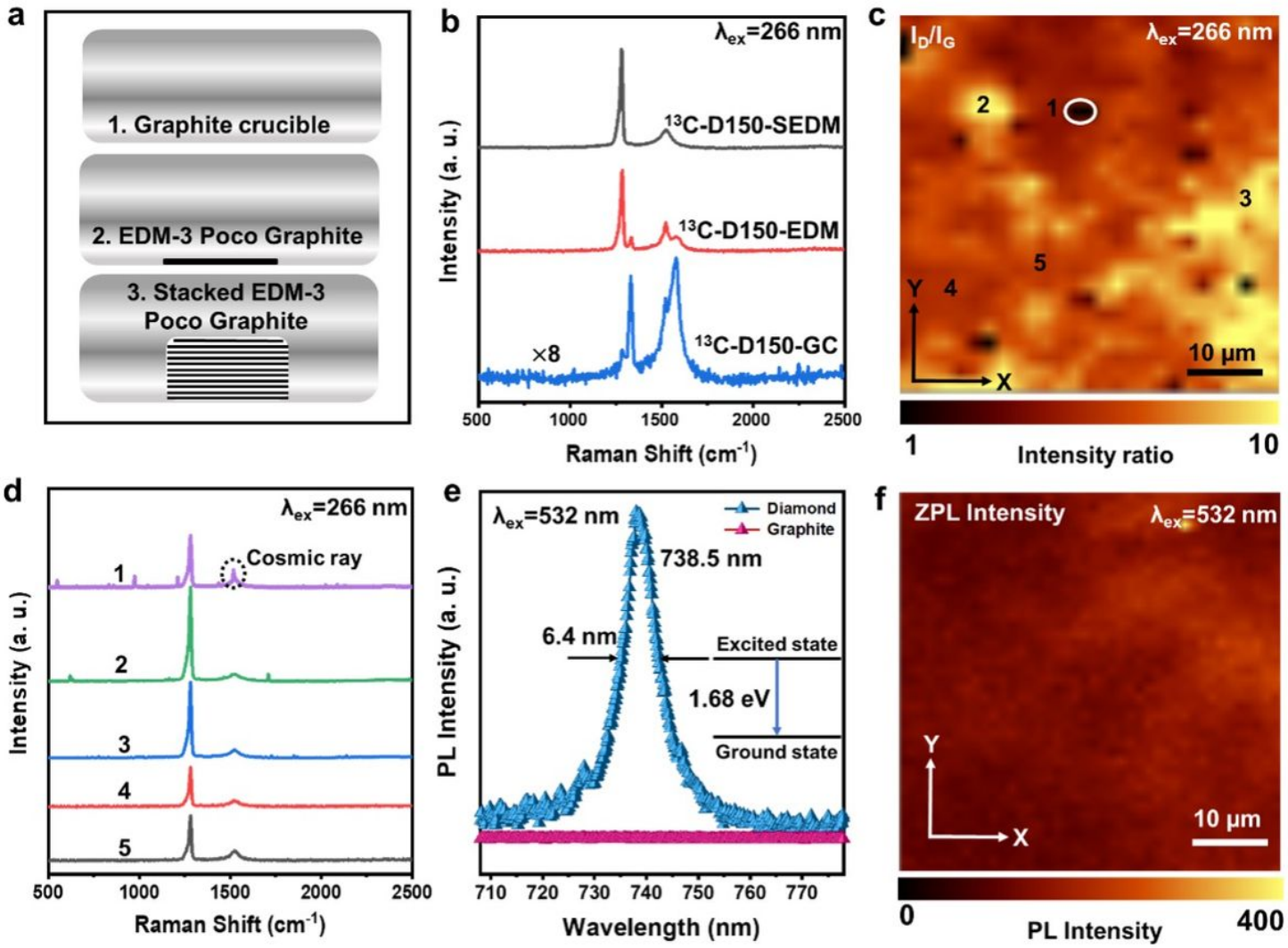

Figure 2

Characterization of ^{13}C-labeled as-grown diamond. (a) Scheme of the three configurations used for growth. (b) Raman spectra of ^{13}C-D150-GC, ^{13}C-D150-EDM, and ^{13}C-D150-SEDM. (c) Raman map of I_D/I_G ratio of the region in ^{13}C-D150-SEDM. (d) Raman spectra taken from the regions marked in (c). (e) ZPL peak of the as-grown diamonds compared to the as-grown graphite, excited by a 532 nm laser. (f) Map of ZPL intensity of ^{13}C-D150-SEDM.

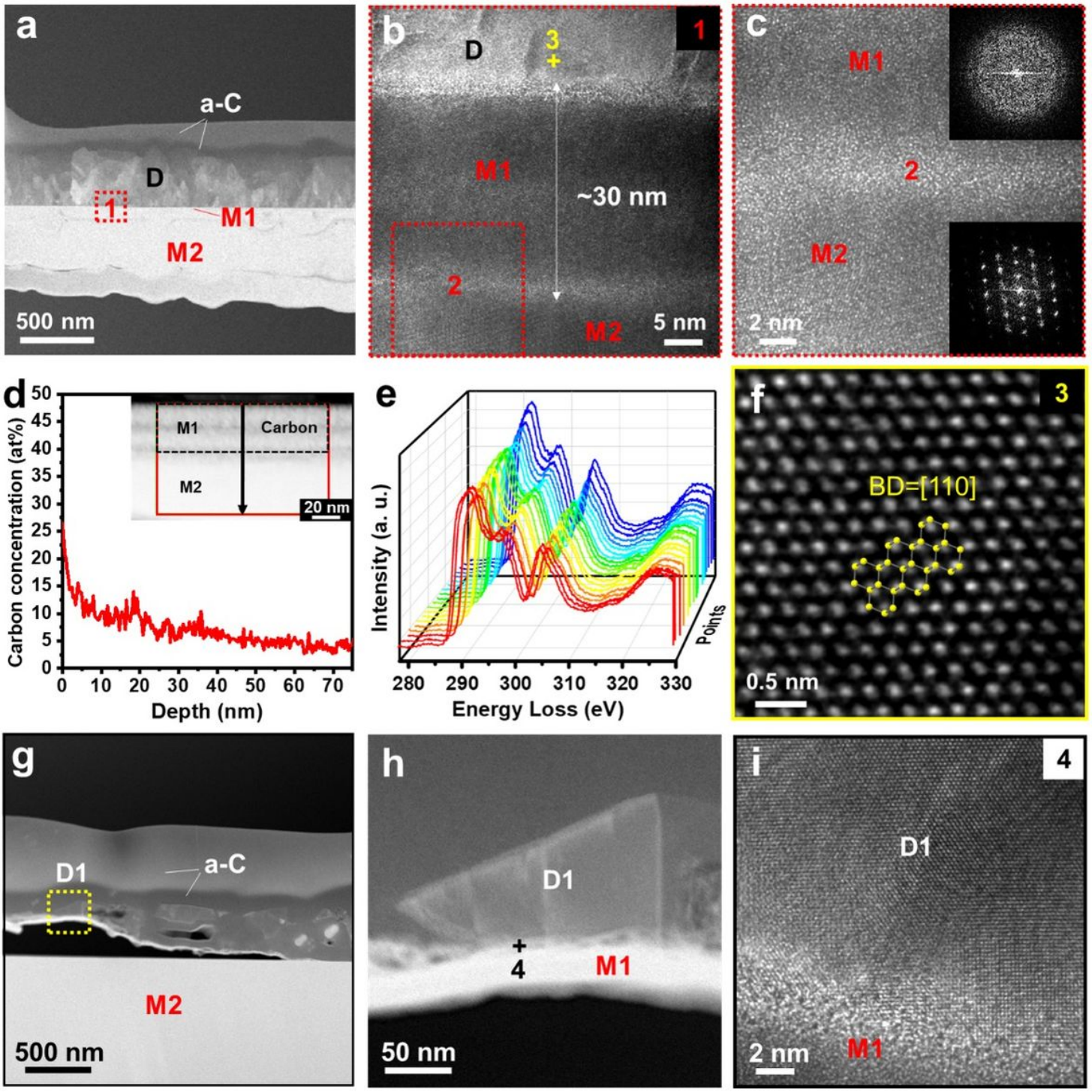

Figure 3

TEM data of cross-section samples prepared by SEM-FIB. (a) Large-area cross-section TEM image of D150 with regions labeled: a-C (amorphous carbon deposited for the SEM-FIB preparation (stabilization layer), D (as-grown diamond film region), M1 (amorphous region present after solidification of liquid metal by rapid cooling), M2 (crystalline region present after solidification of liquid metal by rapid cooling). (b) HR-TEM image of the region enclosed in the red box in (a), which includes D, M1, and M2. (c) HR-TEM image of the region enclosed in the red box in (b). Upper inset: FFT pattern of the M1 region.

Lower inset: FFT pattern of the M2 region. (d) TEM-EDS line profiling showing the carbon concentration of the region containing M1 and M2 of (a). Inset: Corresponding high-angle annular dark-field scanning transmission electron microscopy image showing the TEM-EDS line profiling region. (e) TEM-EELS spectra of the D region in (a). (f) AR-TEM image of the D region indicated by the yellow cross in (b), BD = [110]. (g) Large-area cross-section TEM image of D30 with regions labeled: a-C, D1, M1, and M2 (Note: Some regions of M1 “peel away” from M2 for some of our cross-section samples). (h) TEM images of the regions enclosed in the yellow boxes in (g). (i) HR-TEM images of the regions marked by the black cross in (h).

Supplementary Files

This is a list of supplementary files associated with this preprint. Click to download.

- SupplementalInformationfile.pdf